Observation of new neutron-rich isotopes at the NSCL

Oleg B. Tarasov *

National Superconducting Cyclotron Laboratory, Michigan State University, East Lansing, Michigan 48824, USA

Abstract. Recently, increased primary beam intensities at the National Superconducting Cyclotron Laboratory (NSCL) at Michigan State University and advances in experimental techniques allowed probing further into unknown regions of the table of the isotopes with fragmentation and in-flight fission reactions. Recent measurements at the NSCL have demonstrated that primary beams of ^{48}Ca at 141 MeV/u and ^{76}Ge at 132 MeV/u can be used to produce new isotopes ^{40}Mg, ^{42,43}Al, ^{44}Si, ^{52}Ar, ^{50}Cl, ^{52,53}Ar, ^{55,56}K, ^{57,58}Ca, ^{59,60,61}Sc, ^{62,63}Ti, ^{65,66}V, ^{68}Cr, ^{70}Mn in the proximity of the neutron dripline. Also, experiments with ^{238}U (81 MeV/u) and ^{208}Pb (86 MeV/u) beams in order to measure production yields and possibly observe several neutron rich isotopes in the first time have recently been performed at the NSCL. A search for new neutron-rich isotopes with ^{48}Ca and ^{76}Ge beams was carried out using the recently developed two-stage fragment separator technique.

Keywords: new isotopes; measured cross sections; projectile fragmentation; two-stage separator.
PACS: 27.50.+e,25.70

INTRODUCTION

The discovery of new nuclei in the proximity of the neutron drip line provides a benchmark for nuclear mass models and hence for the understanding of the nuclear force and the creation of elements. Once the production methods and cross sections for the formation of neutron-rich nuclei are understood, further investigations to study the nuclei themselves, such as decay spectroscopy, may be planned. Therefore, the determination of production rates for the most exotic nuclei continues to be an important part of the experimental program at existing and future rare-isotope facilities.

New progress in the production of neutron-rich isotopes is possible given the increased primary beam intensities at the National Superconducting Cyclotron Laboratory (NSCL) at Michigan State University, and advances in experimental techniques allowed probing further into unknown regions of the table of the isotopes with fragmentation and in-flight fission reactions. FRIB secondary beams of neutron-rich isotopes of heavy elements ($Z > 60$) will be important tools in understanding of the nuclear physics of the r-process. Production, identification, and separation of isotopes having $A > 200$ at intermediate energies is one of most challenging and least explored regions.

* On leave from Flerov Laboratory of Nuclear Reactions, JINR, 141980 Dubna, Moscow Region, Russian Federation.

In this work the experiments recently performed at the NSCL and devoted to the first observation of neutron-rich isotopes, reaction mechanism study, and development of technique for future secondary beams are described in chronological order.

^{48}Ca + W,Be

The neutron dripline is only confirmed up to $Z = 8$ (^{24}O) by work at projectile fragmentation facilities [1-4]. Experiments at RIKEN [5] and at GANIL [6] observed the two heaviest isotopes along the $A = 3Z + 4$ line, ^{34}Ne and ^{37}Na, by the fragmentation of ^{48}Ca projectiles. The heavier nuclei in this series, ^{40}Mg and ^{43}Al, were unobserved at that time. All nuclei with $A = 3Z + 3$ up to $Z = 12$ have been shown to be unbound. The neighboring nuclei with $A = 3Z + 2$ have been observed up to ^{41}Al but the production of the heavier nuclei from a ^{48}Ca beam requires a reaction with a net neutron pickup. A series of measurements was carried out at the NSCL to search for new neutron-rich isotopes in this region and to measure the cross sections for production of these isotopes.

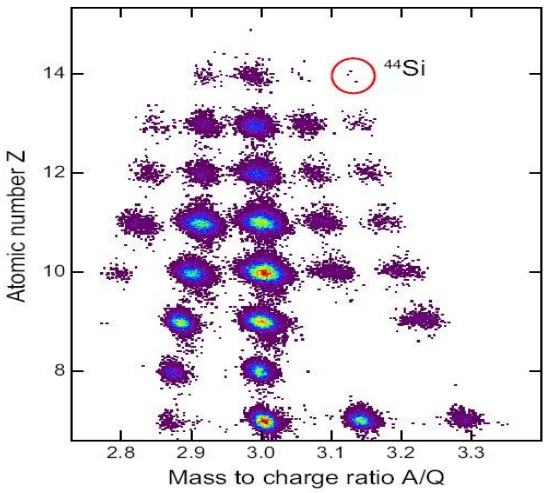

FIGURE 1. Particle identification plot atomic number Z versus mass-to-charge ratio A/Q for $Z = 7$ to 15 of the neutron-rich products, including the new isotope ^{44}Si [8].

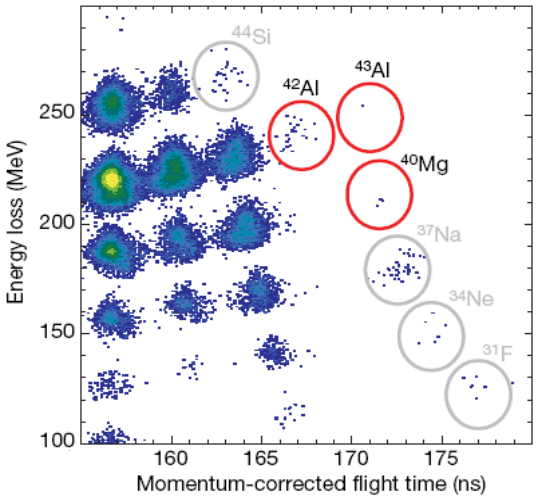

FIGURE 2. Particle identification of the neutron-rich products, including the new isotopes ^{40}Mg, ^{42}Al and the single event identified as ^{43}Al [10].

A 142 MeV/u ^{48}Ca beam from the coupled cyclotron facility was used to irradiate either a ^{9}Be target or a ^{nat}W target located at the normal target position of the A1900 fragment separator [7]. In the experiment to observe ^{40}Mg nuclei with use only the A1900 fragment separator three events identified as ^{44}Si nuclei were observed during the measurements with the tungsten target (see Fig. 1) and none were observed with the beryllium target [8]. This experiment demonstrated that using the A1900 fragment separator as the sole separation stage significantly limits the sensitivity of the experimental setup for very rare isotopes owing to (i) excessive rates and large pile-up probability in the detector located at the intermediate dispersive focal plane of the A1900 fragment separator and (ii) high rates of light nuclei in the final focal plane detectors that cannot be rejected by the energy-loss technique.

The next experiment to search for ^{40}Mg has been done using the combination of the A1900 fragment separator with the S800 analysis beam line [9] to form a two-stage separator [10]. The first stage of the system serves as a selector whereas the second stage contains detectors and functions as analyzer. A search for the most exotic nuclei was carried out with the 707 μm ^{nat}W target for a total of 7.6 days. Three events of ^{40}Mg were clearly identified (see Fig. 2). Further, the 23 events of ^{42}Al establish its discovery. Figure 2 also contains one event consistent with ^{43}Al. The experimental setup is shown in Fig. 3. See work [10] for more details of the experiment, and theoretical predictions of the drip line in this region.

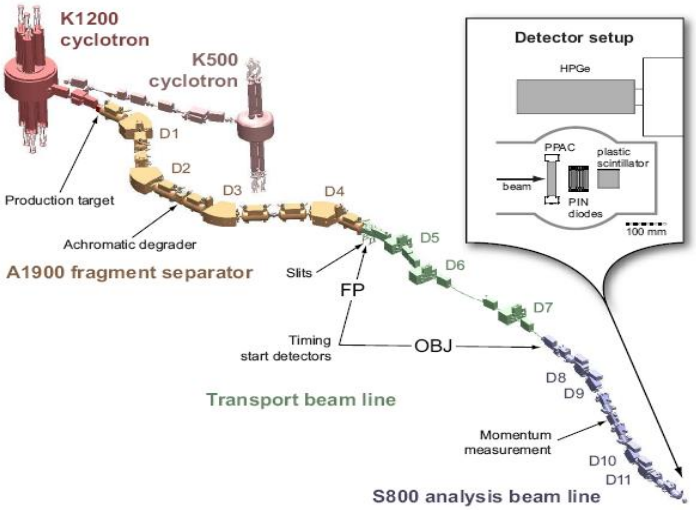

FIGURE 3. Sketch of the experimental setup at the NSCL. This overview diagram shows the equipment used for the production, separation, and detection of new neutron-rich nuclei.

Systematics of the production cross sections of the neutron-rich nuclei

As a starting point, the cross sections in peripheral two-body reactions have been analyzed in the framework of the Q_{gg} systematics for a long time. The central idea of the Q_{gg} systematics is that the products are created in a statistical, thermal process and the cross section should follow the expression:

$$\sigma(Z, A) = f(Z) \exp(Q_{gg} / T), \quad (1)$$

where Q_{gg} is the simple difference between the mass excesses of the ground states of the product and reactant nuclei and T is an effective temperature that is fitted to the data. Projectile fragmentation is usually not described as a two-body process, but rather as a sudden process that forms an excited prefragment followed by statistical decay. Charity [11] has pointed out that the sequential evaporation of light particles from sufficiently excited nuclei follows a general pattern that leads to a somewhat uniform distribution of final products. The separation energies contain the masses of the daughter isotopes, thus, it can be expected an exponential dependence of the yield on the mass difference between the daughter nuclei for proton and neutron emission in this model. A simple systematic framework [8] was found to describe the production cross sections based on thermal evaporation from excited prefragments that allows extrapolation to other weak reaction products by substitution Q_{gg} in Eq. 1 on Q_g, where Q_g is the simple difference between the mass excesses of the ground states of the projectile and the observed fragment. Figure 4 shows the cross sections for the

production of neutron rich nuclei in the reactions ^{48}Ca + Be,Ta,W as a function of the two-body Q values and as a function of the one-body Q value.

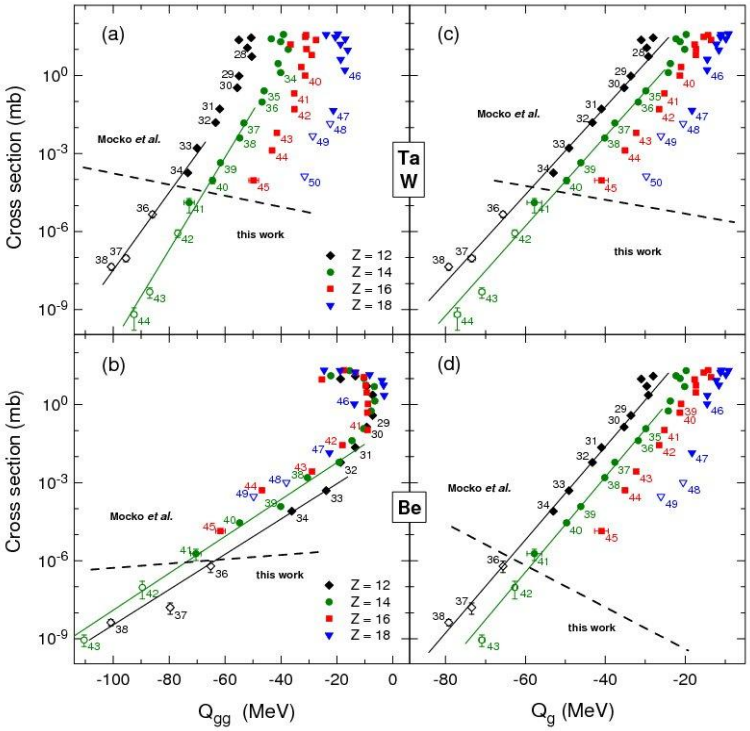

FIGURE 4. The variation [8] of the cross sections for the production of neutron rich nuclei as a function of the two-body Q values [Q_{gg}, left panels (a), (b)] and as a function of the one-body Q value [Q_g, right panels (c), (d)]. Upper panels (a), (c) show data for W (Ta), lower panels (b), (d) for Be targets. Each symbol is labeled with the respective mass number. Data from Ref. [8] (below the dashed lines in each panel) were combined with data from Ref. [12]. Solid symbols represent calculations based on the measured mass values, and open symbols based on the recommended values [13,14]. The lines represent exponential fits of the most neutron-rich isotopes for each chain.

^{238}U + Be

Fission of an 81–MeV/u ^{238}U beam following abrasion by a Be target has been studied at the NSCL [15]. Recoiling fragments were spatially separated from the primary beam and identified using the A1900 fragment separator with magnetic rigidity varied in steps from 2.5–3.9 T m. A search for new neutron-rich nuclides was performed and has shown evidence for production of ^{125}Pd (see Fig. 5). It is necessary to note, that at the same time this isotope has been also observed in RIKEN [16] and GSI [17].

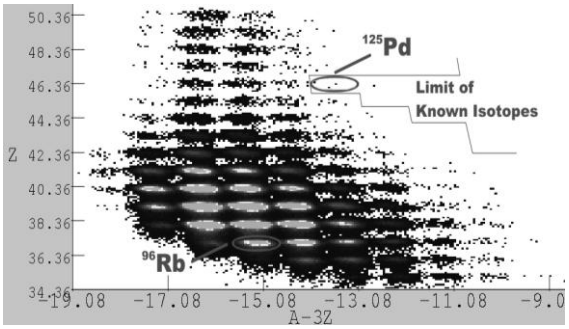

FIGURE 5. Partial identification plot [15] showing measured atomic number Z vs. the calculation function A-3Z for fully stripped ions obtained during a search for new isotopes.

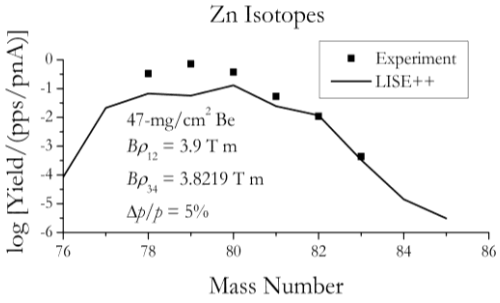

FIGURE 6. Comparison [15] of the observed yield of Zn isotopes produced by in-flight fission of ^{238}U (80MeV/u) to calculations by the LISE^{++} program [18].

The results of measurements showed that many measured yields were in good agreement with those predicted by the LISE^{++} code [18]. For example, Fig. 6 shows the comparison between observed yields of Zn isotopes and LISE^{++} predictions.

In addition to standard particle identification techniques, gamma decays originating from known microsecond isomers were used to provide independent isotopic identification. Finally, eight new microsecond isomeric states in neutron-rich nuclides have been discovered in this experiment [19].

^{208}Pb + Be, Ni

Achieving isotopic identification of A~200 amu should be an important technological development for the Coupled Cyclotron Facility, and in future for the FRIB facility. The theoretical investigation indicates a maximum in the charge-exchange contribution in the case of uranium projectiles in aluminum near 400 MeV/u [20] that may limit an energy loss resolution. More experimental data at lower energies are needed to be conclusive in this statement.

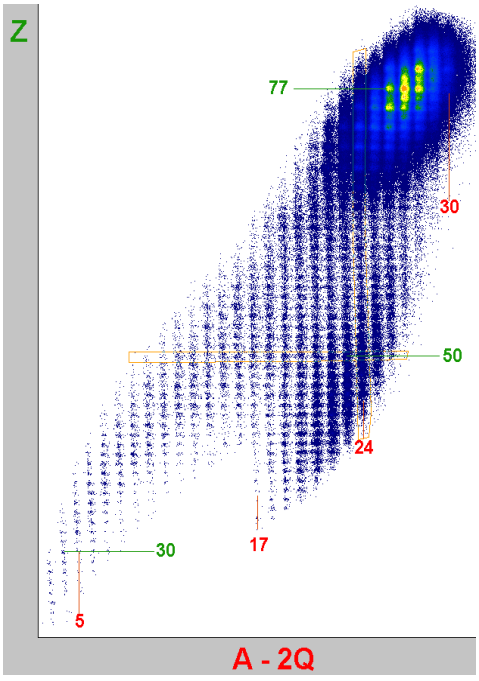

FIGURE 7. Identification plot [21] of fragments produced in the reaction ^{208}Pb(86MeV/u)+Be(9 mg/cm^2) and separated by the A1900 fragment-separator set at the magnetic rigidity 3.1 Tm.

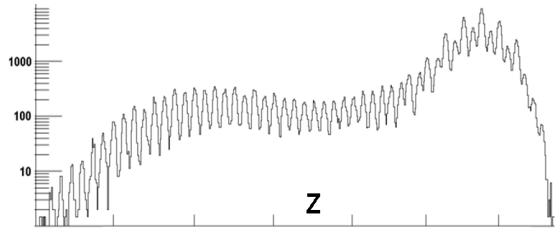

FIGURE 8. Elemental spectra obtained in the experiment NSCL-05120 at the magnetic rigidity of 3.1 Tm.

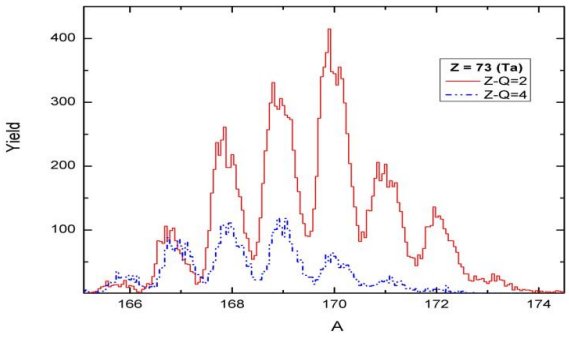

FIGURE 9. Mass distributions of Tantalum isotopes with condition for ionic state Z-Q=2 and 4 at Bρ= 3.1 Tm.

An experiment to obtain A, Z, Q resolution for isotopic and elemental separation in order to measure production yields from a beam of ^{208}Pb (86 MeV/u) on Be and Ni-targets and possibly observe several neutron rich isotopes in the first time has recently been performed at the NSCL [21]. The A1900 fragment-separator was used to analyze products from projectile fragmentation and abrasion-fission. Isotopic identification of

nuclides having $A \sim 200$ has been achieved (see Fig. 7-9), demonstrating that adequate *A*, *Z*, *Q* resolution at this energy region are possible when using the *B*ρ-Δ*E*-*TKE*-*ToF* method and the Si-telescope. The resolution (FWHM) obtained in *A*, *Z* and *Q* for heavy fragments were approximately 0.65, 0.60, and 0.52 units, respectively. The verification of PID is done via detection of multiple charge state distributions of the primary beam, as well as γ-decay of known isomers with half-lives in the microsecond range.

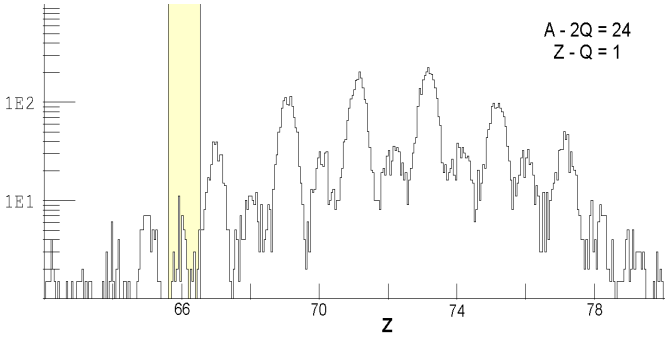

FIGURE 10. Elemental distribution of fragments with conditions for hydrogen-like ions be in the contour *A*-2*Q*=24.

A strong odd-even effect in the yield can be seen to grow as a function of atomic number in Fig. 8. This effect can be observed very clearly in the expanded view (see Fig. 10). Some preliminary calculations indicate that the suppression of even *Z* abrasion-evaporation products might be explained by introducing an odd-even variation of the fission barrier [22], such that even elements are preferentially depleted by fission. LISE^{++} simulations with variation of the fission barrier have been used to explore this hypothesis. Production cross-sections extracted from the data can help improve the accuracy of production models such as Abrasion-Ablation and Abrasion-Fission used in the LISE^{++} code. Also the data [21] reveal the existence of previously unreported isomeric transitions (for example 181 keV in ^{101}Mo).

^{76}Ge + W, Be

The search for new neutron-rich isotopes was carried out [23,24] with a primary beam of ^{76}Ge and using the two-stage fragment separator technique that enabled the discovery of ^{40}Mg and ^{42}Al in 2007 [10] (see Chapter "^{48}CA + W,BE"). A 132 MeV/u ^{76}Ge beam, accelerated by the coupled cyclotrons at the NSCL, was used to irradiate a series of beryllium targets and a tungsten target, each placed at the target position of the A1900 fragment separator.

During all runs, the magnetic rigidity of the last two dipoles was kept constant at 4.3 Tm while the production target thickness was changed to map the fragment momentum distributions. This approach greatly simplified the particle identification during the scans of the parallel momentum distributions. The advantage of this approach—keeping the magnetic rigidity ($B\rho_{0f}$) constant while varying the target thickness—can be seen in Fig. 11, which shows the total distribution of fully stripped reaction products observed in all runs of this work. The range of fragments is shown as the measured atomic number *Z* plotted versus the calculated quantity $A - 3q$. The identification of the individual isotopes in Fig. 11 was confirmed via isomer tagging using the known isomeric decays in ^{32}Al and ^{43}S and from holes in the $A - 3Z = 1$ line corresponding to the unbound nuclei ^{25}O and ^{28}F located between the particle bound nuclei ^{22}N and ^{31}Ne. The details of the calculation of the particle identification are given in the Appendix of Ref. [24]. The observed fragments include 15 new isotopes

that are the most neutron-rich nuclides of the elements chlorine to manganese (^{50}Cl, ^{53}Ar, ^{55,56}K, ^{57,58}Ca, ^{59,60,61}Sc, ^{62,63}Ti, ^{65,66}V, ^{68}Cr, ^{70}Mn). The new neutron-rich nuclei observed in this work are those events to the right of the solid line in Fig. 11 and are indicated by the red squares in Fig. 12.

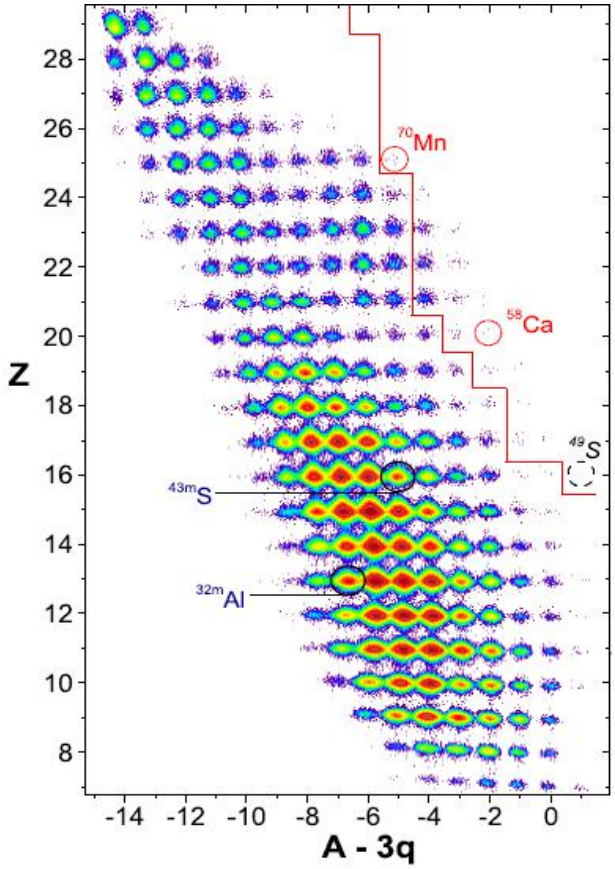

FIGURE 11. Particle identification plot showing the measured atomic number Z vs. the calculated function $A - 3q$ for the nuclei observed in all runs of work [24] (where q is the ionic charge of the fragment). The limit of previously observed nuclei is shown by the solid line as well as the locations of several reference nuclei. Particle identification was confirmed by registering γ rays from short-lived isomeric states of ^{43}S and ^{32}Al (marked by black circles).

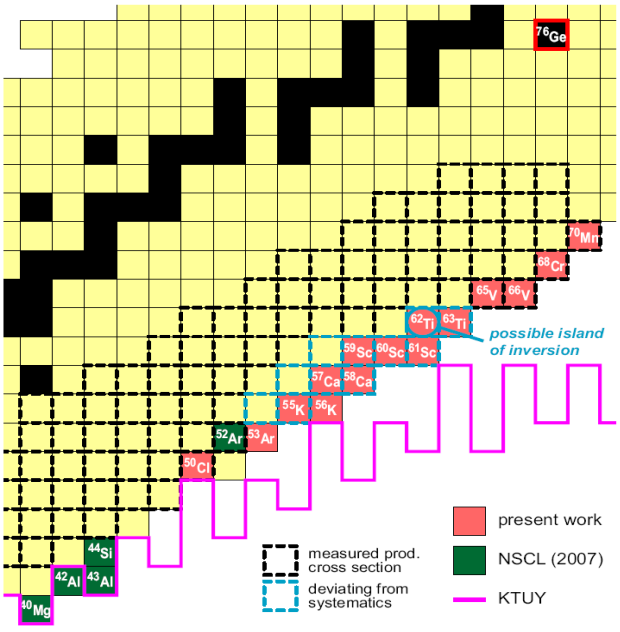

FIGURE 12. The region of the chart of nuclides under investigation [23]. The solid line is the limit of bound nuclei from the KTUY mass model [25]. Nuclei in the green (or dark gray) squares were recently discovered [8,10,26], those in red (or gray) squares are new in this work [23], and the cross sections for those in dashed boxes (production cross sections with Be targets measured in this experiment [23]) are shown in Fig. 13. The center of the new proposed island of inversion at ^{62}Ti [27] is highlighted

New island of inversion?

The production cross sections for the most neutron-rich projectile fragments have been previously shown to have an exponential dependence on Q_g (the difference in mass excess of the beam particle and the observed fragment) [8] (see Chapter "Systematics of the production cross sections of the neutron-rich nuclei"). However, it is important to note that the actual masses of the very neutron-rich nuclei, needed for this calculation, have not been measured and are only available from models. In a shell-model picture, the ground states of nuclei in the new island of inversion near ^{62}Ti [27] (similar to the island of inversion observed near ^{31}Na) would be dominated by intruder configurations corresponding to neutron particle-hole excitations across the $N = 40$ subshell gap into the $g_{9/2}$ [27]. As a test of this suggestion, the cross sections for the production of all nuclei observed with the beryllium and tungsten targets [24] are shown in Fig. 13 where the abscissa, Q_g, is the difference between the mass of the ground state of the projectile and the observed fragment. In this case the masses were taken from Ref. [25]. This empirical mass model (KTUY) provides an excellent systematization of the variation of the data, with the logarithm of the cross sections for each isotopic chain falling on an approximately straight line. Nearly all the data from the beryllium targets can be fitted with the single value of $T = 1.8$ MeV,

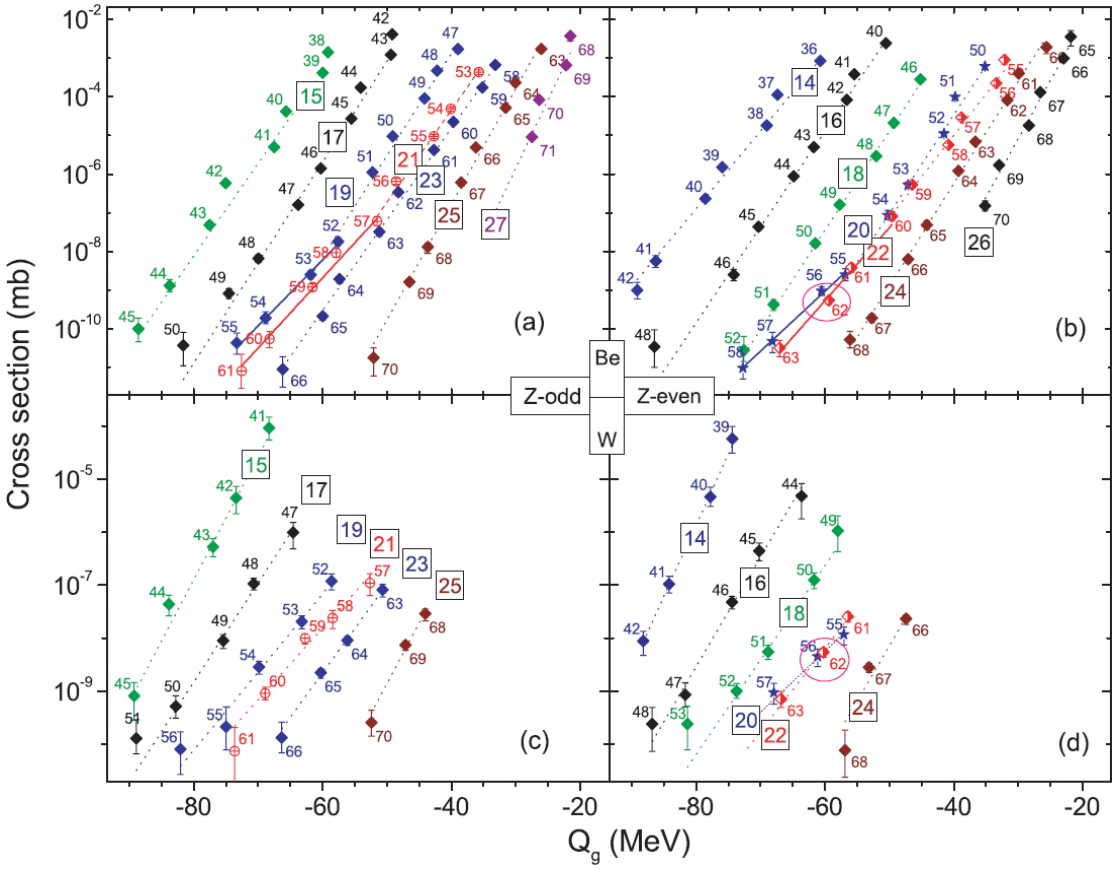

FIGURE 13. Cross sections [24] for the production of neutron-rich nuclei with (a, c) odd atomic numbers and (b, d) even atomic numbers, with (a, b) a beryllium target and (c, d) a tungsten target, respectively. See text for explanation of the lines. The cross sections for ^{62}Ti at the center of the proposed new island of inversion [27] are circled.

but slightly better fits are obtained by finding the optimum T for each element. However, the heaviest isotopes of elements in the middle of the distribution (Z = 19, 20, 21, and 22) appear to break away from the straight-line behavior. These heaviest four or five isotopes of these elements were found to have a shallower slope (shown by the solid lines) or enhanced cross sections relative to the model prediction. Recall that the masses of these most neutron-rich nuclei are not fit in the model but are extrapolated. This might indicate that these nuclei are more bound (i.e., less negative Q_g) than current mass models predict. One reason for a stronger binding can be deformation. In a shell-model framework, functions of the ground and low-lying excited states of nuclei in the new island of inversion around ^{62}Ti would be dominated by neutron particle-hole intruder excitations across the N = 40 subshell gap, leading to deformation and shape coexistence.

The systematic variation of the production cross sections as a function of Qg was checked with several other well-known mass models and essentially the same behavior was observed. Specifically, models based on the Hartree-Fock-Bogoliubov method, HFB-8, HFB-9 [28], and the very recent HFB-17 version [29], the finite range droplet model (FRDM) [30], and the 2003 Atomic Mass Evaluation (AME2003) [13] with shell-crossing corrections that were developed in the LISE^{++} framework [14] were found to give similar results The different behavior of the calcium isotopes with the beryllium target can be seen more clearly in Fig. 14. The same effect is present in the same mass region with the tungsten target.

The variation of the individual fitted values of the inverse slope parameter, T , for products from both targets is shown as a function of atomic number in Fig. 15. The inverse slopes of the cross sections from the beryllium target connected by dashed (solid) lines in Fig. 13 are indicated by the half-filled black diamonds and dashed lines (the filled circles and solid lines) in Fig. 15. Similar for the tungsten target the inverse slopes are shown by the open red triangles connected by dotted lines, but the range of cross sections was more limited and only one slope parameter was fitted to their data. Figure 15 clearly shows that there is a general increase in T for all of the heavy isotopes observed with Z = 19, 20, 21, and 22.

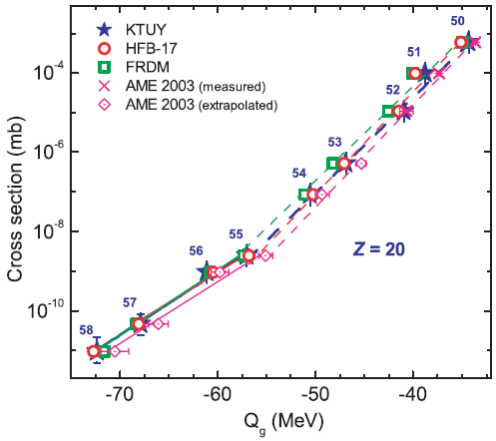

FIGURE 14. Production cross sections of neutron-rich calcium isotopes with a beryllium target [24] as a function of Q_g calculated with different mass models.

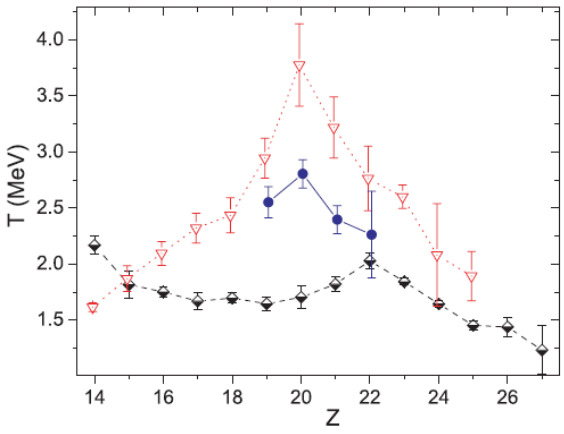

FIGURE 15. Values of the inverse slope parameter [24], T , to the experimental cross sections in Fig. 13 shown as a function of atomic number. See text for details.

Parallel momentum distributions

Being able to predict the momentum distributions of residues when searching for new isotopes is important in order to optimize the fragment separator for the production of the most exotic isotopes. Also, accurate modeling of the momentum distributions allows for an estimation of the transmission and efficient suppression of contaminants. In projectile fragmentation, the common way of measuring the momentum distributions of the fragments is to scan the magnetic rigidity ($B\rho$) with a fragment separator. A thin target is generally used to avoid complications from differential energy loss in the target (the systematic change in the kinetic energy lost by the projectile and residue nuclei in the target). A new approach to measure momentum distributions and cross sections (called "target scanning") is presented in Ref. [31]. In contrast to the so called "$B\rho$ scanning" method, typically using one thin target, a variety of targets with different thicknesses were used with a constant magnetic rigidity in the separator. In the case of very neutron-rich isotopes with low production, the "$B\rho$ scanning" method with a thin target is unpractical, whereas the "target scanning" method is particularly well suited to survey neutron-rich reaction residues. At a magnetic rigidity setting corresponding to the production of heavy neutron-rich nuclei, the lighter fragments have higher yields but will experience the largest differential energy loss, and hence, will fall outside the momentum acceptance of the separator with the thicker targets.

The longitudinal momentum distributions of 34 neutron-rich isotopes of elements produced by fragmentation of a ^{76}Ge beam at 132 MeV/u with $13 \leq Z \leq 27$ were scanned [24] using a novel experimental approach [31] where a variety of targets with different thicknesses was used with the fragment separator at constant magnetic rigidity. Although the convolution model [33] gives a good agreement for the fragment velocities, the calculated widths are narrower than experimentally observed. The formulae used in the convolution model are too complicated to fit the experimental data due to the large number of parameters. In comparison to models that describe the shape and centroid of fragment momentum distributions, a parametrization based on the measured data was derived. A survey of all of the fitted results shows that fragments in the heavy mass region are produced with significantly higher velocities and slightly broader momentum distributions than the Morrissey model [32] predictions. This model assumes that the energy necessary to remove each nucleon is $E_S = 8$ MeV, a value derived for fragments close to stability. Neutron-rich nuclei are less bound, which could explain their higher velocities than compared to stable nuclei. The separation energy parameter for nuclei observed in work in the region $A_P/2 \leq A_F \leq A_P$ exhibits a linear decrease with the number of removed nucleons:

$$E_S = 8 - 11.2\Delta A / A_P; \qquad (2)$$

where $\Delta A = A_P - A_F$, A_P is the projectile mass number, and A_F is the fragment mass number. The reduced width parameter [32] has been estimated $\sigma_0 = 105 \pm 15$ MeV/c. Details the of transmission calculations, the analysis of their uncertainties, as well as the general analysis of momentum distributions and deduced cross sections obtained with this approach are presented in Ref. [33].

ACKNOWLEDGMENTS

I would like to acknowledge, also on behalf of the investigators of discussed experiments [8,10,15,19,21,23,24,31], the operations staff of the NSCL for providing the intense ^{48}Ca, ^{76}Ge, ^{208}Pb, and ^{238}U beams necessary for these studies. This work was supported by the U.S. National Science Foundation under grant PHY-06-06007.

REFERENCES

1. D. Guillemaud-Mueller et al., Phys. Rev. C **41**, 937 (1990).
2. M. Fauerbach et al., Phys. Rev. C **53**, 647 (1996).
3. O. Tarasov et al., Phys. Lett. B **409**, 64 (1997).
4. H. Sakurai et al., Phys. Lett. B **448**, 180 (1999).
5. M. Notani et al., Phys. Lett. B **542**, 49 (2002).
6. S. M. Lukyanov et al., J. Phys. G **28**, L41 (2002).
7. D. J. Morrissey et al., Nucl. Instrum. Methods Phys. Res. B **204**, 90 (2003).
8. O. B. Tarasov et al., Phys. Rev. C **75**, 064613 (2007).
9. D. Bazin et al., Nucl. Instrum. Methods Phys. Res. B **204**, 629 (2003).
10. T. Baumann et al., Nature **449,** 1022 (2008).
11. R. J. Charity, Phys. Rev. C **58**, 1073 (1998).
12. M. Mocko et al., Phys. Rev. C **74**, 054612 (2006).
13. G. Audi, A. H.Wapstra, and C. Thibault, Nucl. Phys. A729, 337 (2003).
14. O. B. Tarasov and D. Bazin, Tech. Rep. MSUCL1248, NSCL, Michigan State University (2002).
15. C.M. Folden III et al., in Proceedings of the Fourth International Conference on Fission and Properties of Neutron-Rich Nuclei, World Scientific, Singapore, 2008, p. 426.
16. T.Ohnishi et al.,J.Phys.Soc.Jpn. **77**, 83201 (2008).
17. J.Benlliure, et al., Phys.Rev. C **78**, 054605 (2008).
18. O. B. Tarasov, D. Bazin, Nucl. Inst. Meth. Phys. Res. B 266 (2008) 4657; LISE^{++} code available at: http:\\www.nscl.msu.edu\lise
19. C.Folden III et al., Phys.Rev. C **79**, 064318 (2009).
20. H.Weick et al., Nucl. Inst. Meth. Phys. Res. B **193**, 1 (2002).
21. O. B. Tarasov et al., Nuclear Physics (to be submitted).
22. A. J. Sierk, Phys. Rev. C **33**, 2039 (1986).
23. O.B. Tarasov et al., Phys.Rev.Lett. **102**, 142501 (2009).
24. O.B. Tarasov et al., Phys. Rev. C, **80**, 034609 (2009).
25. H. Koura et al., Prog. Theor. Phys. **113**, 305 (2005).
26. P. F. Mantica et al., Bull. Am. Phys. Soc. **53**, 64 (2008).
27. B.A. Brown, Prog. Part. Nucl. Phys. **47**, 517 (2001).
28. M. Samyn, S. Goriely, and J. M. Pearson, Nucl. Phys. A **725**, 69 (2003).
29. S. Goriely, N. Chamel, and J. M. Pearson, Phys. Rev. Lett. **102**, 152503 (2009).
30. P. Moller et al., At. Data Nucl. Data Tables **59**, 185 (1995).
31. O.B. Tarasov et al., NIM A, submitted (2009).
32. D. J. Morrissey, Phys. Rev. C 39, **460** (1989).
33. O. Tarasov, Nucl. Phys. A **734**, 536 (2004).